Published in final edited form as:

Kidney Int. 2016 January ; 89(1): 95–104. doi:10.1038/ki.2015.315.

Raloxifene improves skeletal properties in an animal model of cystic chronic kidney disease

Christopher L. Newman[1], **Amy Creecy**[2], **Mathilde Granke**[3,4], **Jeffry S. Nyman**[3,4], **Nannan Tian**[5], **Max A. Hammond**[6], **Joseph M. Wallace**[6,7], **Drew M. Brown**[1], **Neal Chen**[8], **Sharon M. Moe**[8,9], and **Matthew R. Allen**[1,8]

[1]Department of Anatomy and Cell Biology, Indiana University School of Medicine, Indianapolis, IN

[2]Department of Biomedical Engineering, Vanderbilt University, Nashville, TN

[3]Department of Orthopaedic Surgery and Rehabilitation and Vanderbilt Center for Bone Biology, Vanderbilt University Medical Center, Nashville, TN

[4]Department of Veterans Affairs, Tennessee Valley Healthcare System, Nashville, TN

[5]Materials Engineering, Purdue University, West Lafayette, IN

[6]Weldon School of Biomedical Engineering, Purdue University, West Lafayatte, IN

[7]Department of Biomedical Engineering, Indiana University—Purdue University, Indianapolis, IN

[8]Division of Nephrology, Department of Medicine, Indiana University School of Medicine, Indianapolis, IN

[9]Roudebush VA Medical Center, Indianapolis, IN

Abstract

Patients with chronic kidney disease (CKD) have an increased risk of fracture. Raloxifene is a mild anti-resorptive agent that reduces fracture risk in the general population. Here we assessed the impact of raloxifene on the skeletal properties of animals with progressive CKD. Male Cy/+ rats that develop autosomal dominant cystic kidney disease were treated with either vehicle or raloxifene for five weeks. They were assessed for changes in mineral metabolism and skeletal parameters (microCT, histology, whole bone mechanics, and material properties). Their normal littermates served as controls. Animals with CKD had significantly higher parathyroid hormone levels compared to normal controls as well as inferior structural and mechanical skeletal properties. Raloxifene treatment resulted in lower bone remodeling rates and higher cancellous bone volume in the rats with CKD. While it had little effect on cortical bone geometry it resulted in higher energy to fracture and modulus of toughness values than vehicle-treated rats with CKD, achieving levels equivalent to normal controls. Animals treated with raloxifene had superior

Send Correspondence to: Matthew R. Allen, PhD, Dept. of Anatomy and Cell Biology, MS 5035, Indiana University School of Medicine, 635 Barnhill Dr., Indianapolis, IN 46202, Tel: 317-274-1283, FAX: 317-278-2040, ; Email: matallen@iupui.edu

DISCLOSURES

The authors have no conflicts of interest related to the described work.

tissue-level mechanical properties as assessed by nanoindentation and higher collagen D-periodic spacing as assessed by atomic force microscopy. Thus, raloxifene can positively impact whole bone mechanical properties in CKD through its impact on skeletal material properties.

Keywords

chronic kidney disease; bone quality; raloxifene

INTRODUCTION

Chronic kidney disease—mineral and bone disorder (CKD-MBD) is characterized by hyperphosphatemia, secondary hyperparathyroidism, and an increased risk of fractures [1–3]. For patients with early stage CKD (estimated glomerular filtration rate greater than 30 mL/min) and normal PTH levels, most guidelines adopt treatment recommendations for osteoporosis patients without CKD [3–4]. The majority of patients with osteoporosis are treated with anti-resorptive agents that reduce osteoclast-mediated bone loss [5]. Unfortunately, the complex metabolic background of CKD and a lack of clinical data in patients with advanced disease have limited the use of these agents.

Raloxifene is a selective estrogen receptor modulator with mild anti-resorptive properties. Clinical trials have shown that it effectively reduces fracture risk in patients with osteoporosis despite modest reductions in bone turnover and meager improvements in bone volume, mineralization, and BMD [6–7]. Preclinical studies indicate that raloxifene improves mechanical properties through its effects on bone quality [8–10]. Specifically, raloxifene positively affects bone toughness (the ability of bone to tolerate damage without fracturing). This improvement occurs in the absence of significant changes in bone mass [8–9] and appears to be partly due to changes in bone matrix hydration [11–12]. Furthermore, secondary analyses of a human clinical trial have revealed beneficial renal outcomes in patients using raloxifene [13]. Preclinical experiments [14–15] and a small clinical study in dialysis patients [16] have supported these findings. Taken together, these data suggest that raloxifene could have beneficial effects on several consequences of CKD. The goal of the current work was to test the hypothesis that raloxifene would improve skeletal properties in an animal model of progressive CKD.

RESULTS

Mineral Metabolism

Animals with CKD had higher serum levels of BUN compared to normal littermates (+231%), consistent with previous data indicating the presence of late stage kidney disease (estimated to be 20–25% of normal kidney function) (Table 1). Serum calcium was normal, while phosphorus (+48%), FGF23 (+266%), and PTH levels (+1106%) were all significantly higher than their normal counterparts. Raloxifene-treated animals had biochemical profiles that were statistically indistinguishable from their untreated CKD counterparts although non-significant trends existed for PTH, phosphorous and FGF23.

MicroCT

Vehicle-treated CKD animals had lower trabecular bone volume (with lower trabecular number and higher trabecular spacing) relative to normal animals at the proximal tibia. Raloxifene had normal trabecular bone volume in the proximal tibia (due to higher trabecular number and lower spacing than CKD animals) (Figure 1 and Table 2). In the vertebra, CKD animals had significantly lower trabecular bone volume (due to lower trabecular number and higher spacing) compared to normal controls. Raloxifene-treated animals had an intermediate phenotype, with BV/TV higher than vehicle-treated CKD animals but still lower than normal controls (Figure 1 and Table 2).

Cortical bone of the femoral midshaft was also negatively affected by CKD. CKD animals had lower cortical area, cortical thickness, and cross-sectional moments of inertia compared to normal controls (Table 2). There was no difference in cortical porosity between normal and vehicle-treated CKD animals. Raloxifene treatment resulted in less porosity than CKD animals but displayed no differences in cortical area, thickness, or moments of inertia. CKD animals had thinner vertebral cortices than their normal counterparts, and raloxifene animals were similar to vehicle-treated animals (Table 2).

Histology

Vehicle-treated CKD animals had higher trabecular bone formation rates in the tibia (+137%) and vertebra (+306%) compared to normal animals (Figure 2). This was a result of higher mineral apposition rates as well as a higher proportion of mineralizing surfaces (Table 3). Animals with CKD also had higher osteoclast number and percent osteoclast surface than their normal counterparts (Table 3). Raloxifene animals had lower bone formation rates compared to vehicle-treated CKD animals at both the tibia and the vertebra; these rates were not different from normal controls (Figure 2). Osteoclast parameters were similar in vehicle-treated CKD animals and their raloxifene-treated counterparts (Table 3).

Whole Bone Mechanics

Animals with CKD had lower femoral cortical bone ultimate force (−25%), stiffness (−22%), and energy to fracture (−23%) compared to normal animals (Figure 3 and Table 4). Estimated material properties revealed a significantly lower modulus of toughness in CKD animals (−16%) (Figure 3). Ultimate stress and elastic modulus were not different (Table 4). Animals treated with raloxifene displayed a higher energy to fracture compared to vehicle-treated CKD animals accompanied by higher (though not normal) ultimate force. There was no effect of treatment on stiffness. There also was no effect of raloxifene treatment on ultimate stress or elastic modulus, but the modulus of toughness was equivalent to normal (Figure 3).

Vertebral compression tests revealed that CKD animals had lower ultimate force and energy to ultimate force but no differences in stiffness compared to normal animals (Figure 3 and Table 4). There also was no effect on estimated material properties of the vertebra. Compared to animals with CKD, raloxifene had no impact on any structural or estimated material properties in the vertebra.

Bone Material Properties

Based on nanoindentation and AFM indentation, CKD-vehicle animals had indistinguishable material properties from the normal controls (Table 5). Raloxifene treatment resulted in harder skeletal tissue (assessed by nanoindentation) compared to both normal and CKD-vehicle animals (Table 5). Tissue composition (assessed by Raman spectroscopy) and collagen crosslinking (assessed by HPLC) revealed no differences among the three groups (Table 6). Collagen D-periodic spacing was not affected by CKD, but animals treated with raloxifene had higher D-periodicity in the collagen fibrils compared to CKD animals (Figure 4). NMR spectroscopic measures revealed no differences among groups for bound or free water (Table 6).

DISCUSSION

This experiment shows that in the setting of progressive CKD with high bone turnover, raloxifene treatment leads to lower tibial and vertebral trabecular bone remodeling. More importantly, energy to fracture and the modulus of toughness at the femoral diaphysis were higher in animals treated with raloxifene than their CKD counterparts. Nanoindentation also revealed that raloxifene treatment led to substantially harder cortical bone, while AFM imaging of collagen D-periodic spacing detected raloxifene-specific effects. Collectively, these data demonstrate that raloxifene can benefit skeletal material properties (those independent of bone mass) as well as structural properties and that together these ameliorate some of the CKD-associated deficits in whole bone mechanical properties.

Animals with CKD had substantially higher bone formation rates than their normal counterparts, indicating that untreated CKD animals have high turnover bone disease. Raloxifene effectively suppressed the high turnover induced by CKD to the level that was not significantly different than normal animals. While consistent with clinical data in postmenopausal women [17], this normalization of bone remodeling is in contrast to previous work in the same model using bisphosphonates and calcium, both of which suppressed remodeling in trabecular bone to well below normal levels [18–19]. Due to concerns over the dramatic suppression of bone remodeling in patients with CKD, the level of suppression observed with raloxifene may be advantageous. On the other hand, osteoclast number and percent osteoclast surface remained high in tibial trabecular bone with raloxifene treatment. This lack of effect on osteoclasts is consistent with biopsy data from postmenopausal women treated with raloxifene for two years [17]. Although raloxifene is typically associated with suppressed osteoclast formation, reduced osteoclast activity without a reduction in number has been described in other studies as well [20–21]. In this model of hyperparathyroidism, high levels of PTH may actually overshadow raloxifene's effect on osteoclast formation, making its effect on the activity of mature osteoclasts more pronounced.

Untreated CKD animals had compromised mechanical properties of the long bones, consistent with previous studies in this model [18,22]. Raloxifene normalized energy to fracture, restoring it to the level of normal animals. Estimated material properties indicate that raloxifene specifically improved material-level toughness. These effects were absent in the vertebra. Because vertebral compression testing ceases at the ultimate load, information

regarding effects on whole bone and material-level toughness are limited, likely the reason for the no effect on these properties. Nevertheless, the positive effects of raloxifene on long bone mechanical properties represent the first study in this animal model in which a treatment has returned bone properties to normal levels in the absence of other adverse effects.

Though bone material properties can be estimated from whole bone mechanical tests, more direct assessments of cortical bone material properties were conducted at various length scales to better understand what aspects of bone quality raloxifene impacted in CKD bone. Unlike previous studies examining cortical bone mechanics in these animals [23], changes in material properties due to CKD were not apparent in this study. These data also contrast with changes in elastic modulus and hardness observed in the trabecular bone of patients with high turnover CKD [24]. However, because rodents do not display intracortical remodeling, high turnover is primarily a trabecular phenomenon in rodent models of CKD. Despite no obvious changes in cortical bone material properties in this study, raloxifene still had positive effects on hardness as measured by nanoindentation. Previous studies in murine and ovine ovariectomy models have also shown raloxifene-induced improvements in hardness [25–26]. While it is not clear how improving material-level hardness influences the modulus of toughness and energy to fracture, these results have been observed several times in animals treated with raloxifene [8–9,11,25–26].

Among the various components of bone quality, changes in hydration have been established as having significant effects on the mechanical properties of bone [27]. Previous studies have revealed that raloxifene improvements in material properties are associated with higher bound water in the extracellular matrix [11–12]. The current NMR data are inconsistent with these previous data because they revealed no effect on bound water in raloxifene-treated animals. The reason for this discrepancy is unclear. For example, CKD-associated changes in bone metabolism may prevent raloxifene from impacting bound water in these animals. Differences in animal models (dogs were used in previous studies) may be a factor as well. These differences may also reflect variations in the magnetic resonance techniques employed across these studies [11–12].

Rather than changes in hydration, the current work showed that raloxifene increased collagen fibril spacing (D-periodicity). Changes in collagen structure have been linked to altered bone mechanical properties [28]. Though the exact contribution of D-periodicity to whole bone mechanical properties remains unclear, this effect is consistent with previous work using raloxifene [11]. Previous studies have shown decreased D-periodic spacing in animals with reduced energy to fracture [29–30]. Hence, this work improves the current understanding of D-periodicity by showing that increases in D-periodicity are associated with improved bone toughness.

Consistent with our previous studies [18,22,31], animals with CKD had drastically higher levels of PTH than their normal counterparts. This occurred in the presence of normal calcium and phosphorus levels. Though Cy/+ rats eventually become hypocalcemic and hyperphosphatemic [18,31], the animals in this study only displayed the earlier rise in PTH observed in late stage CKD [2]. While no significant treatment effects were noted, trends

were observed towards higher PTH and lower FGF23. While raloxifene's impact on PTH may have affected bone outcomes, specific details regarding its mechanism cannot be determined from the current work. Unfortunately, the current literature has provided mixed results regarding the relationship between raloxifene and estrogen on serum PTH in the setting of hyperparathyroidism [32–37]. Clearly, more work is necessary to understand the interplay between raloxifene and serum biochemistry in the setting of CKD-MBD.

Most clinical data examining raloxifene's use in CKD are derived from secondary assessments of large clinical trials, where they retrospectively examined patients with mild CKD [38]. Like their osteoporosis counterparts, CKD patients treated with raloxifene had a lower rate of vertebral fractures as well as increased BMD at the hip and spine. Far fewer data exist for patients with late stage disease due to their exclusion from osteoporosis trials. One small study examined BMD in patients on dialysis and showed that raloxifene improved BMD in the spine but not in the hip [16]. Another study examined BMD at the distal radius and found that raloxifene improved BMD in patients with mild hyperparathyroidism [33]. Despite these data, there have been no assessments of fracture efficacy using raloxifene in CKD. Because the current study suggests significant mechanical benefits despite modest changes in bone mass, the positive effects of raloxifene may be overlooked if BMD alone is used to determine efficacy.

Hesitation exists about raloxifene's use in CKD mainly because of concerns about the increased risk of thromboembolism [4]. Post-hoc analyses of clinical CKD data with raloxifene show that the risk was not worse than the general population [13]. Previous guidelines have actually highlighted the need for further research using raloxifene in CKD, encouraging clinical trials examining safety and efficacy outcomes (including fracture incidence and vascular calcifications) [3]. The current results support those recommendations prior to the broad translation of this drug into clinical practice. Such studies will need to be undertaken in both sexes to ensure that our results in male Cy/+ rats translate to both males and females with CKD. Most importantly, such studies must include assessments beyond BMD in order to truly assess its efficacy in these patients. Recent techniques assessing bone quality have been developed for and examined in humans (ultrashort echo time magnetic resonance imaging [39] and reference point indentation [40–41]). These, alongside BMD, may provide a better picture of the potential efficacy of raloxifene in patients with advanced kidney disease.

In light of these benefits, a few limitations must be acknowledged. The current duration of treatment approximated only one remodeling cycle in rats. Hence, the long-term effects of raloxifene in this model are unknown. Also, Cy/+ rats provide a model of high turnover CKD and may not translate to models of low turnover bone disease. Finally, because rodents do not undergo intracortical remodeling, future work will need to assess the mechanical benefits of raloxifene in an animal model of CKD with intracortical remodeling.

In summary, the current study shows that CKD rats treated with raloxifene had lower bone turnover and superior whole bone mechanical properties than their vehicle-treated counterparts. These beneficial effects on whole bone properties appear to be due to localized material property improvements. Because these changes occurred mostly independently of

changes in bone mass, traditional methods to evaluate efficacy in CKD bone disease may be insufficient for the evaluation of raloxifene in these patients.

METHODS

Animal Model

Cy/+ rats are characterized by autosomal dominant cystic disease [42]. These animals have a mutation (R823W) in *Anks6*, a gene that codes for the protein SamCystin. The function of this protein is unknown [43], but unlike many other cyst-related proteins, SamCystin does not localize to the primary cilia of kidney cells [44]. Recently, this gene was shown to be responsible for nephronophthisis in humans [45]. In this rat model, the mutation leads to a slow and gradual onset of CKD [42]. It parallels the human condition through the gradual development of abnormal mineral homeostasis and vascular calcification. Blood urea nitrogen (BUN) and creatinine are elevated by 25 weeks of age. At 30 weeks, kidney function is about 25% of that observed in normal animals, leading to progressive hyperphosphatemia, hyperparathyroidism, and skeletal abnormalities.

Experimental Design

Male Cy/+ rats were identified as in previous studies using this model [46–47]. Their normal littermates (n=8) served as controls. At 24 weeks, animals were placed on a casein diet (Purina AIN-76A; 0.7% Pi, 0.6% Ca) to increase phosphorus availability. This diet has been shown to produce a more consistent kidney disease phenotype [42].

Starting at 25 weeks of age, Cy/+ rats were treated with vehicle (n=9) or raloxifene (n=10) (1 mg/kg daily; subcutaneous) for 5 weeks. This treatment duration was chosen as it approximates an average bone remodeling cycle in skeletally mature rats (roughly six months in humans) and has been shown to be sufficient to detect treatment-induced skeletal changes in this model [18,22]. Raloxifene doses were based upon previous studies in ovariectomized female rats [10]. All rats were injected with calcein (10 mg/kg; subcutaneous) 14 and 4 days prior to sacrifice to label surfaces with actively forming bone.

At 30 weeks of age, animals were anesthetized with isoflurane and underwent cardiac puncture for blood draw followed by exsanguination and bilateral pneumothorax to ensure death. The lumbar spine, tibiae, and femora were removed and stored at −20°C for analysis. All procedures were approved by and carried out according to the rules and regulations of the Indiana University School of Medicine’s Institutional Animal Care and Use Committee.

Biochemistry

Blood plasma at 30 weeks was analyzed for BUN, calcium, and phosphorus using colorimetric assays (Point Scientific, Canton, MI, or Sigma kits). Intact PTH was determined by ELISA (Alpco, Salem, NH), which had an intra-assay CV of 4.8% and an inter-assay CV of 3.2%. FGF23 was assessed with a two-site assay (Immunotopics, San Clemente, CA) [18,31].

Micro-Computed Tomography (microCT)

Using microCT (Skyscan 1172), trabecular bone volume (BV/TV, %) and architecture (number, spacing, and thickness) were determined from trabecular bone isolated from the metaphysis of the proximal tibia and the entire L4 vertebra. Cortical bone geometry (area, thickness, bending moments of inertia, and porosity) was determined from the femoral midshaft. Cortical thickness was assessed at 75% of the height of the vertebra (from cranial to caudal) because this represents a region free of zygapophyseal attachment. All bones were wrapped in parafilm to prevent drying and scanned at a resolution of 12 μm in accordance with standard guidelines [48].

Histomorphometry

Static and dynamic histomorphometric measures were obtained from the proximal metaphysis of the left tibia and the caudal metaphysis of the L3 vertebra. Histological processing followed previously used protocols [49–51]. Tissues were embedded in methyl methacrylate for undecalcified sections. Mid-transverse sections (4 μm) of cancellous bone from the proximal tibia and the caudal portion of the L3 vertebra were cut and left unstained for dynamic histomorphometry or stained with tartrate-resistant acid phosphatase (TRAP) for osteoclast measurements (tibia only). For tibial and vertebral cancellous bone, a region of interest (encompassing 7–8 mm^2 and 1.5–2.0 mm^2, respectively) approximately 0.8 mm from the growth plate was analyzed. The unstained sections were assessed for total bone surface, single-labeled surface, and double-labeled surface to calculate mineral apposition rate (MAR), percent mineralizing surface (MS/BS), and bone formation rate (BFR/BS). Because previous work in this model displayed no change in osteoid with disease, those measures were not conducted in this experiment. TRAP-stained sections were assessed for bone surface, osteoclast number, and osteoclast surface to calculate the number of osteoclasts per unit bone surface (N.Oc/BS) and percent osteoclast surface (Oc.S/BS). All histomorphometric nomenclature follows standard usage [52]. Six samples (two from each group) contained no double label and were excluded from MAR and BFR/BS calculations.

Whole Bone Mechanics

Structural mechanical properties of the left femur were determined by four-point bending. The anterior surface was placed on two lower supports located ±9 mm from the mid-diaphysis (18 mm span length) with an upper span length of 6 mm. Specimens were loaded to failure at a rate of 2 mm/min, producing a force-displacement curve for each sample. Structural mechanical properties (ultimate force, stiffness, energy to fracture, total displacement) were obtained directly from these curves, while apparent material properties (ultimate stress, elastic modulus, toughness) were derived from the force-displacement curves, cross-sectional moments of inertia (I_{ml}), and the distances from the centroid to the tensile surface using standard beam-bending equations for four-point bending [53].

Structural mechanical properties of the L4 vertebra were determined by uniaxial compression. Vertebra height was assessed from microCT images. Prior to mechanical testing, the vertebral arch and endplates were removed using an Isomet saw to create parallel surfaces (inside the growth plates) for compression testing. One untreated CKD sample was damaged during processing and thus not used for testing. Specimens were loaded at a rate of

0.5 mm/min, producing a force-displacement curve for each sample. Structural mechanical properties were obtained directly from these curves, while apparent material properties were derived from the force-displacement curves, pre-test sample heights, and the average bone area of five microCT slices (10%, 30%, 50%, 70%, and 90% slices of the pre-test sample height) using standard equations for uniaxial compression [54–55].

Tissue Composition

The anteromedial portion of the right tibial mid-diaphysis was polished with a 0.05 μm alumina suspension in order to create a flat region for spectroscopy and subsequent indentation testing. Raman spectroscopy was performed using a LabRAM HR 800 Raman Spectrometer (HORIBA JobinYvon, Edison, NJ) connected to a BX41 microscope (Olympus, Tokyo, Japan). A 660 nm laser was focused on the bone surface using a 50X objective to a spot size of ~10 μm. Three locations were imaged ~3 mm apart on the polished surface with five 20 second acquisitions at each location as previously published [56]. A five-point linear baseline correction was applied in LabSpec 5 (HORIBA JobinYvon). Using OriginPro 8.6 (OriginLab, Northampton, MA), a single Gaussian peak was fit to the PO_4^{3-}ν1 peak, and the areas under the PO_4^{3-}ν1 (930–980 cm^{-1}), CO_3^{2-}ν1 (1056–1091 cm^{-1}), and Amide I (1551–1720 cm^{-1}) bands were calculated at each location. Type B carbonate substitution was found by the band area ratio of CO_3^{2-}ν1/PO_4^{3-}ν1. The degree of matrix mineralization was determined by the band area ratio of PO_4^{3-}ν1/Amide I. Mineral maturity (crystallinity) was determined by the inverse of the full width at half maximum (FWHM) of the PO_4^{3-}ν1 peak.

AFM Indentation

Using the polished tibial surface described above, indentations were performed using a BioScope Catalyst atomic force microscope (Bruker, Santa Barbara, CA), operating in peak force tapping mode using previously published methods [57]. Samples were partially submerged in ultrapure water with the surface remaining uncovered for optical imaging of the surface in order to determine indentation locations but then fully submerged during testing. Indentations were performed using a tungsten carbide-coated AFM probe (Nanotec; nominal tip radius of 60 nm) with a nominal spring constant of 650 N/m. Three locations (co-localized with Raman measurements) per sample were indented, and at each location (20 μm×20 μm grid), 100 indentations were performed. Samples were loaded to 3.25 μN with force-separation curves acquired from each indentation. Within each location, indentations were spaced about 2 μm apart in order to avoid interactions from neighboring indentations. In total, 300 indentations were performed for each sample. The indentation elastic modulus was calculated from 20% to 80% of the withdrawal curve using the Sneddon model of contact between a rigid cone and an elastic half space because the indentation depth is greater than the radius of curvature of the probe [57]. Only those indentations whose retraction curve produced an r^2 value of 0.90 or higher were included in the analysis (n=6–95 per location). The indentation elastic modulus was determined from the following equation:

$$F = \frac{2}{\pi} \cdot \frac{E_s}{1-\upsilon_s} \cdot \tan\alpha \cdot \delta^2$$

where F is the indentation force, E_S is the indentation elastic modulus of the sample, ν_S is the Poisson's ratio of the sample (assumed to be 0.35), α is the opening angle (assumed to be 20°), and δ is the indentation depth. All of the individual indentations were averaged to produce a single value for each location, and each of these locations was averaged to produce a single value for each sample.

Nanoindentation

After AFM indentation, nanoindentation was performed on the same tibial samples using a Hysitron TI950 TriboIndenter. As above, samples were partially submerged in ultrapure water with the surface remaining uncovered for optical imaging of the surface in order to determine indentation locations but then fully submerged during testing. Three locations (co-localized with AFM indentations) per sample were indented. Pre-saved test locations were imaged using the nanoindenter for *in situ* scanning probe imaging. Within this imaged region, 6 indentations were performed on a 10 μm × 20 μm grid. Indentations were spaced 10 μm apart in order to avoid interactions from neighboring indentations. A previously calibrated fluid cell Berkovich diamond probe was used for the indentations. Machine calibrations were performed at the beginning of each day of testing. Tests were conducted in load control, and the loading profile consisted of a 10s loading period, a 10s hold at 3000 μN, and a 10 s unloading period. From the resulting load-displacement profiles, the indentation elastic modulus and hardness were calculated according to the following equations:

$$E_r = \frac{\sqrt{\pi}}{2\sqrt{A(h_c)}} \cdot S$$
$$H = \frac{P_{max}}{A(h_c)}$$

where E_r is the reduced indentation elastic modulus of the sample, A is contact area, h_c is the contact displacement, S is the stiffness of the sample determined from 40–95% of the unloading slope, H is the hardness of the sample, and P_{max} is the peak force. All of the individual indentations (n=6 per location) were averaged to produce a single value for each location, and each of these locations was averaged to produce a single value for each sample.

Collagen Morphology

Following indentation testing, the polished tibial surface was partially decalcified by soaking the bones in 0.5 M EDTA for 25 minutes followed by five minutes of sonication in a water bath. This process was repeated five times for each sample. For imaging, RTESPA probes were used (Bruker; nominal radius of 8 nm; spring constant = 40 N/m). For measurements of collagen morphology, the scan size was set at 3.5 μm with 512×512 pixels and a scan rate of 0.5 lines/s. Two locations between indentation sites were imaged per sample (one location was dropped from a raloxifene sample due to poor image quality), and 12 fibrils were measured at each location. All 24 fibrils were averaged to produce a single value for each

animal (one normal sample had only 18 fibrils and two CKD samples had 14 and 20 fibrils due to poor image quality). Using SPIP 5.1.10 (Image Metrology, Hørsholm, Denmark), D-periodic spacing was calculated using 2D Fast Fourier Transformations as previously described [57].

Collagen Cross-Linking

After four-point bending, proximal segments of the left femoral cortex (~3 mm in length) were fully demineralized in 20% EDTA (0.68 M, pH 7.4). Approximately 10 mg of demineralized bone were hydrolyzed in 6N HCl (~10 μL per 1 mg) at 110°C for 20–24 hours. After evaporating the acid using a SpeedVAC centrifuge with a cold trap, each hydrolysate was resuspended in ultrapure water, split into two equal portions, and dried. Half of the residue was resuspended in ultrapure water with an internal standard (5×10^{-6} g/L pyridoxine). The solution was filtered and diluted with 0.05% heptafluorobutyric acid in 10% acetonitrile, and 50 μL of each hydrolysate were assayed by a high performance liquid chromatography (HPLC) system (Beckman-Coulter System Gold 168) with a silica-based column (Waters Spherisorb) as previously published [58]. Standards with varying concentrations of pyridinoline (PYD; Quidel), deoxypyridinoline (DPD; Quidel), pentosidine (PE; International Maillard Reaction Society), and a constant amount of pyridoxine were also assayed. Using a Waters 2475 fluorescence detector (excitation/emission of 295/400 nm for PYD and DPD and 328/378 nm for PE), chromatograms were recorded to determine the amount of each crosslink. These amounts were then normalized by collagen content, which was determined from the other half of each hydrolysate by another HPLC assay. With α-amino-butyric acid (α-ABA) included as an internal standard, the amino acids were subjected to derivatization with phenyl isothiocyanate (PITC). Along with varying concentrations of derivatized hydroxyproline (Sigma) and a constant amount of α-ABA as standards, the derivatized samples were resuspended in a buffer solution of 5% acetonitrile in 5 mM disodium phosphate. Upon injecting 50 μL of this sample, chromatograms were generated with a UV detector (Beckman-Coulter System Gold 168). The calculated mass of hydroxyproline was then multiplied by 7.5 (assuming 13–14% of type I collagen by mass) and divided by the molecular weight of collagen (30,000 Da), thereby giving crosslink concentration as mol/mol of collagen.

^{1}H Nuclear Magnetic Resonance Spectroscopy

A ~5-mm cross-section of the left femoral mid-shaft was placed into a low proton, loop-gap-style radio-frequency (RF) coil along with a reference microsphere of water (T_2~2 s). As previously published [58], the nuclear magnetic resonance spectroscopy (NMR) analysis was performed in a 4.7-T horizontal-bore magnet (Varian Medical Systems, Santa Clara, CA) using 90°/180° RF pulses of ~9/18-μs duration and collecting Carr-Purcell-Meiboom-Gill (CPMG) measurements with 10,000 echoes at 100 μs spacing in order to separate proton signals within the bone. To generate the spectrum of transverse relaxation time constants (T_2), the echo magnitudes were fitted with multiple exponential decay functions. Upon normalizing the integrated areas of bound water (T_2=1200–800 μs) and pore water (T_2=800 μs –600 ms) to the area of the reference (T_2=600 ms–10 s), the volume of bound water and the volume of pore water were divided by the specimen volume (calculated using Archimedes' principle) to give bound water (bw) and pore water (pw) volume fractions.

Statistics

Comparisons among groups were assessed by one-way ANOVA with Fisher's LSD post-hoc tests. For parameters with non-normal distributions (assessed by Shapiro-Wilk tests), comparisons among groups were made by Kruskal-Wallis tests with Mann-Whitney U post-hoc tests (using a Bonferroni correction). The specific test used for each variable is noted in the figures/tables. *A priori* α-levels were set at 0.05 to determine significance. Data are presented as mean ± standard deviation.

Acknowledgments

This work was supported by the National Institutes of Health grants DL100093 (CLN), AR063157 (JSN), and AR58005 (SMM) and the Indiana Clinical and Translational Sciences Institute grant TR000162 (CLN). The cross-linking analysis was supported using resources and facilities at the VA Tennessee Valley Healthcare System. The authors would like to thank Shannon Roy for technical assistance. They would also like to acknowledge the late Dr. Vincent H. Gattone II (1951–2013) for his instrumental work in developing and maintaining the animal model employed in the current study.

References

1. Levey AS, Eckardt KU, Tsukamoto Y, Levin A, Coresh J, Rossert J, Zeeuw D, Hostetter TH, Lameire N, Eknoyan G. Definition and classification of chronic kidney disease: a position statement from Kidney Disease Improving Global Outcomes (KDIGO). Kidney Int. 2005; 67:2089–2100. [PubMed: 15882252]
2. Levin A, Bakris GL, Molitch M, Smulders M, Tian J, Williams LA, Andress DL. Prevalence of abnormal serum vitamin D, PTH, calcium, and phosphorus in patients with chronic kidney disease: results of the study to evaluate early kidney disease. Kidney Int. 2007; 71:31–38. [PubMed: 17091124]
3. KDIGO . Clinical practice guidelines for the management of CKD–MBD. Kidney Int. 2009; 76:S1–S130.
4. Ott SM. Therapy for patients with CKD and low bone mineral density. Nat Rev Nephrol. 2013; 9:681–692. [PubMed: 24100401]
5. McClung M, et al. Bisphosphonate therapy for osteoporosis: benefits, risks, and drug holiday. Am J Med. 2013; 126:13–20. [PubMed: 23177553]
6. Ettinger B, et al. Reduction of Vertebral Fracture Risk in Postmenopausal Women With Osteoporosis Treated With Raloxifene: Results From a 3-Year Randomized Clinical Trial. JAMA. 1999; 282:637–645. [PubMed: 10517716]
7. Reginster JY. Antifracture efficacy of currently available therapies for postmenopausal osteoporosis. Drugs. 2011; 71:65–78. [PubMed: 21175240]
8. Allen MR, et al. Raloxifene enhances material-level mechanical properties of femoral cortical and trabecular bone. Endocrinology. 2007; 148:3908–3913. [PubMed: 17478550]
9. Allen MR, et al. Raloxifene enhances vertebral mechanical properties independent of bone density. Bone. 2006; 39:1130–1135. [PubMed: 16814622]
10. Diab T, et al. Effects of the combination treatment of raloxifene and alendronate on the biomechanical properties of vertebral bone. J Bone Miner Res. 2011; 26:270–276. [PubMed: 20687153]
11. Gallant, et al. Bone cell-independent benefits of raloxifene on the skeleton: A novel mechanism for improving bone material properties. Bone. 2014; 61:191–200. [PubMed: 24468719]
12. Allen, et al. In vivo UTE-MRI Reveals Positive Effects of Raloxifene on Skeletal Bound Water in Skeletally Mature Beagle Dogs. J Bone Miner Res. 2015; doi: 10.1002/jbmr.2470
13. Melamed ML, et al. Raloxifene, a selective estrogen receptor modulator, is renoprotective: a post-hoc analysis. Kidney Int. 2011; 79:241–249. [PubMed: 20927038]
14. Dixon A, et al. Renoprotective effects of a selective estrogen receptor modulator, raloxifene, in an animal model of diabetic nephropathy. Am J Nephrol. 2011; 27:120–128. [PubMed: 17308373]

15. Zhang Y, et al. Raloxifene modulates estrogen-mediated B cell autoreactivity in NZB/W F1 mice. J Rheumatol. 2010; 37:1646–1657. [PubMed: 20551107]
16. Hernandez E, et al. Effects of raloxifene on bone metabolism and serum lipids in postmenopausal women on chronic hemodialysis. Kidney Int. 2003; 63:2269–2274. [PubMed: 12753317]
17. Ott SM, Oleksik A, Lu Y, Harper K, Lips P. Bone histomorphometric and biochemical marker results of a 2-year placebo-controlled trial of raloxifene in postmenopausal women. J Bone Miner Res. 2002; 17:341–348. [PubMed: 11811565]
18. Moe SM, Chen NX, Newman CL, Gattone VH II, et al. A comparison of calcium to zoledronic acid for improvement of cortical bone in an animal model of CKD. J Bone Miner Res. 2014; 29:902–910. [PubMed: 24038306]
19. Moe SM, Radcliffe JS, White KE, Gattone VH II, Seifert MF, Chen X, Aldridge B, Chen NX. The pathophysiology of early-stage chronic kidney disease–mineral bone disorder (CKD-MBD) and response to phosphate binders in the rat. J Bone Miner Res. 2011; 26:2672–2681. [PubMed: 21826734]
20. Prestwood KM, Gunness M, Muchmore DB, Lu Y, Wong M, Raisz LG. A comparison of the effects of raloxifene and estrogen on bone in postmenopausal women. J Clin Endocrinol Metab. 2000; 85:2197–2202. [PubMed: 10852452]
21. Taranta A, et al. The selective estrogen receptor modulator raloxifene regulates osteoclast and osteoblast activity in vitro. Bone. 2002; 30:368–376. [PubMed: 11856644]
22. Allen MR, Chen NX, Gattone VH II, Chen X, Carr AJ, LeBlanc P, Brown D, Moe SM. Skeletal effects of zoledronic acid in an animal model of chronic kidney disease. Osteoporos Int. 2013; 24:1471–1481. [PubMed: 22907737]
23. Newman CL, Moe SM, Chen NX, et al. Cortical Bone Mechanical Properties Are Altered in an Animal Model of Progressive Chronic Kidney Disease. PLoS ONE. 2014; 9:e99262. [PubMed: 24911162]
24. Malluche HH, et al. Differences in bone quality in low- and high-turnover renal osteodystrophy. J Am Soc Nephrol. 2012; 23:525–532. [PubMed: 22193385]
25. Brennan TC, Rizzoli R, Ammann P. Selective modification of bone quality by PTH, pamidronate, or raloxifene. J Bone Miner Res. 2009; 24:800–808. [PubMed: 19063681]
26. Burket JC, et al. Variations in nanomechanical properties and tissue composition within trabeculae from an ovine model of osteoporosis and treatment. Bone. 2013; 52:326–336. [PubMed: 23092698]
27. Granke M, Does MD, Nyman JS. The role of water compartments in the material properties of cortical bone. Calcif Tissue Int. 2015; 97:292–307. [PubMed: 25783011]
28. Garnero P. The role of collagen organization on the properties of bone. Calcif Tissue Int. 2015; 97:229–240. [PubMed: 25894071]
29. Wallace JM, et al. Distribution of type I collagen morphologies in bone: relation to estrogen depletion. Bone. 2010; 46:1349–1354. [PubMed: 19932773]
30. Bart ZR, Hammond MA, Wallace JM. Multi-scale analysis of bone chemistry, morphology and mechanics in the oim model of osteogenesis imperfecta. Connect Tissue Res. 2014; 55:4–8. [PubMed: 25158170]
31. Moe SM, et al. Anti-sclerostin antibody treatment in a rat model of progressive renal osteodystrophy. J Bone Miner Res. 2015; 30:539–549.
32. Haghverdi F, Mortaji S, Soltani P, Saidi N, Farbodara T. Effect of raloxifene on parathyroid hormone in osteopenic and osteoporotic postmenopausal women with chronic kidney disease stage 5. Iran J Kidney Dis. 2014; 8:461–466. [PubMed: 25362221]
33. Tanaka M, Itoh K, Matsushita K, Matsushita K, Moriishi M, Kawanishi H, Fukagawa M. Effects of raloxifene on bone mineral metabolism in postmenopausal Japanese women on hemodialysis. Ther Apher Dial. 2011; 15(Suppl 1):62–66. [PubMed: 21595855]
34. Saito O, Saito T, Asakura S, Akimoto T, Inoue M, Ando Y, Muto S, Kusano E. Effects of raloxifene on bone metabolism in hemodialysis patients with type 2 diabetes. Int J Endocrinol Metab. 2012; 10:464–469. [PubMed: 23843805]

35. Rubin MR, Lee KH, McMahon DJ, Silverberg SJ. Raloxifene lowers serum calcium and makers of bone turnover in postmenopausal women with primary hyperparathyroidism. J Clin Endocrinol Metab. 2003; 88:1174–1178. [PubMed: 12629102]
36. Zanchetta JR, Bogado CE. Raloxifene reverses bone loss in postmenopausal women with mild asymptomatic primary hyperparathyroidism. J Bone Miner Res. 2001; 16:189–190. [PubMed: 11149484]
37. Carillo-Lopez N, et al. Indirect regulation of PTH by estrogens may require FGF23. J Am Soc Nephrol. 2009; 20:2009–2017. [PubMed: 19628670]
38. Ishani A, et al. The effect of raloxifene treatment in postmenopausal women with CKD. J Am Soc Nephrol. 2008; 19:1430–1438. [PubMed: 18400939]
39. Techawiboonwong A, et al. Cortical bone water: in vivo quantification with ultrashort echo-time MR imaging. Radiology. 2008; 248:824–833. [PubMed: 18632530]
40. Diez-Perez A, et al. Microindentation for in vivo measurement of bone tissue mechanical properties in humans. J Bone Miner Res. 2010; 25:1877–1885. [PubMed: 20200991]
41. Farr JN, et al. In vivo assessment of bone quality in postmenopausal women with type 2 diabetes. J Bone Miner Res. 2014; 29:787–795. [PubMed: 24123088]
42. Moe SM, Chen NX, Seifert MF, Sinders RM, Duan D, Chen X, Liang Y, Radcliff JS, White KE, Gattone VH II. A rat model of chronic kidney disease-mineral bone disorder. Kidney Int. 2009; 75:176–184. [PubMed: 18800026]
43. Nagao S, Morita M, Kugita M, Yoshihara D, et al. Polycystic kidney disease in Hab:SPRD Cy rats is associated with elevated expression and mislocalization of SamCystin. Am J Physiol Renal Physiol. 2010; 299:F1078–F1086. [PubMed: 20719982]
44. Stagner EE, Bouvrette DJ, Cheng J, Bryda EC. The polycystic kidney disease-related proteins Bicc1 and SamCystin interact. Biochem Bioph Res Co. 2009; 383:16–21.
45. Hoff S, et al. ANKS6 is a central component of a nephronophthisis module linking NEK8 to INVS and NPHP3. Nat Genet. 2013; 45:951–956. [PubMed: 23793029]
46. Cowley BD Jr, Grantham JJ, Muessel MJ, Kraybill AL, et al. Modification of disease progression in rats with inherited polycystic kidney disease. Am J Kidney Dis. 1996; 27:865–879. [PubMed: 8651252]
47. Cowley BD Jr, Rupp JC, Muessel MJ, Gattone VH II. Gender and the effect of gonadal hormones on the progression of inherited polycystic kidney disease in rats. Am J Kidney Dis. 1997; 29:265–272. [PubMed: 9016899]
48. Bouxsein ML, et al. Guidelines for assessment of bone microstructure in rodents using micro-computed tomography. J Bone Miner Res. 2010; 25:1468–1486. [PubMed: 20533309]
49. Allen MR, Follet H, Khurana M, Sato M, Burr DB. Antiremodeling agents influence osteoblast activity differently in modeling and remodeling sites of canine rib. Calcified Tissue Int. 2006; 79:255–261.
50. Allen MR, Erickson AM, Wang X, Burr DB, Martin RB, Hazelwood SJ. Morphological assessment of basic multicellular unit resorption parameters in dogs shows additional mechanisms of bisphosphonate effects on bone. Calcified Tissue Int. 2010; 86:67–71.
51. Allen MR, Kubek DJ, Burr DB. Cancer treatment dosing regimens of zoledronic acid result in near-complete suppression of mandible intracortical bone remodeling in beagle dogs. J Bone Miner Res. 2010; 25:98–105. [PubMed: 19580463]
52. Dempster, et al. Standardized nomenclature, symbols, and units for bone histomorphometry: A 2012 update of the report of the ASBMR Histomorphometry Nomenclature Committee. J Bone Miner Res. 2013; 28:2–17. [PubMed: 23197339]
53. Turner, CH.; Burr, DB. Experimental techniques for bone mechanics. In: Cowin, SC., editor. Bone Mechanics Handbook. Boca Raton: CRC Press; 2002.
54. Hogan H, Ruhmann S, Sampson H. The mechanical properties of cancellous bone in the proximal tibia of ovariectomized rats. J Bone Miner Res. 2000; 15:284–292. [PubMed: 10703930]
55. Bloomfield S, Allen M, Hogan H, Delp M. Site- and compartment-specific changes in bone with hindlimb unloading in mature adult rats. Bone. 2002; 31:149–157. [PubMed: 12110428]

56. Hammond MA, Gallant MA, Burr DB, Wallace JM. Nanoscale changes in collagen are reflected in physical and mechanical properties of bone at the microscale in diabetic rats. Bone. 2014; 60:26–32. [PubMed: 24269519]

57. Wallace JM. Applications of atomic force microscopy for the assessment of nanoscale morphological and mechanical properties of bone. Bone. 2012; 50:420–427. [PubMed: 22142635]

58. Allen, et al. Changes in skeletal collagen cross-links and matrix hydration in high- and low-turnover chronic kidney disease. Osteoporosis Int. 2015; 26:977–985.

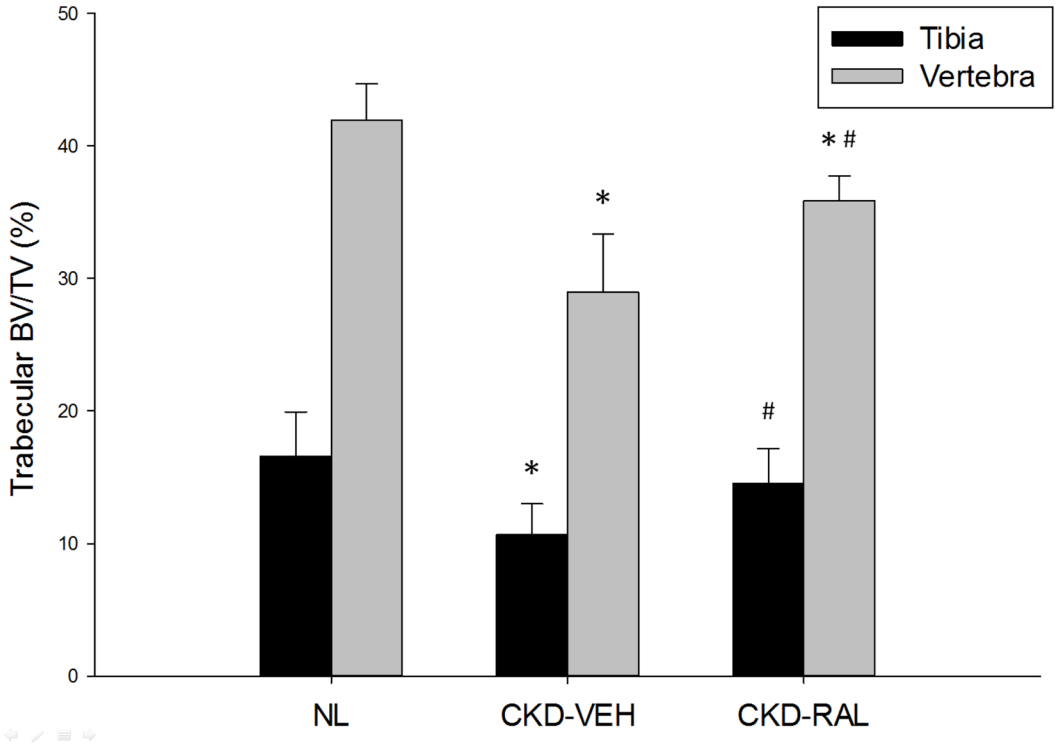

Figure 1.

Cancellous bone structure in the proximal tibia and lumbar vertebra as determined by microCT. *, $p<0.05$ compared to NL; #, $p<0.05$ compared to CKD-VEH

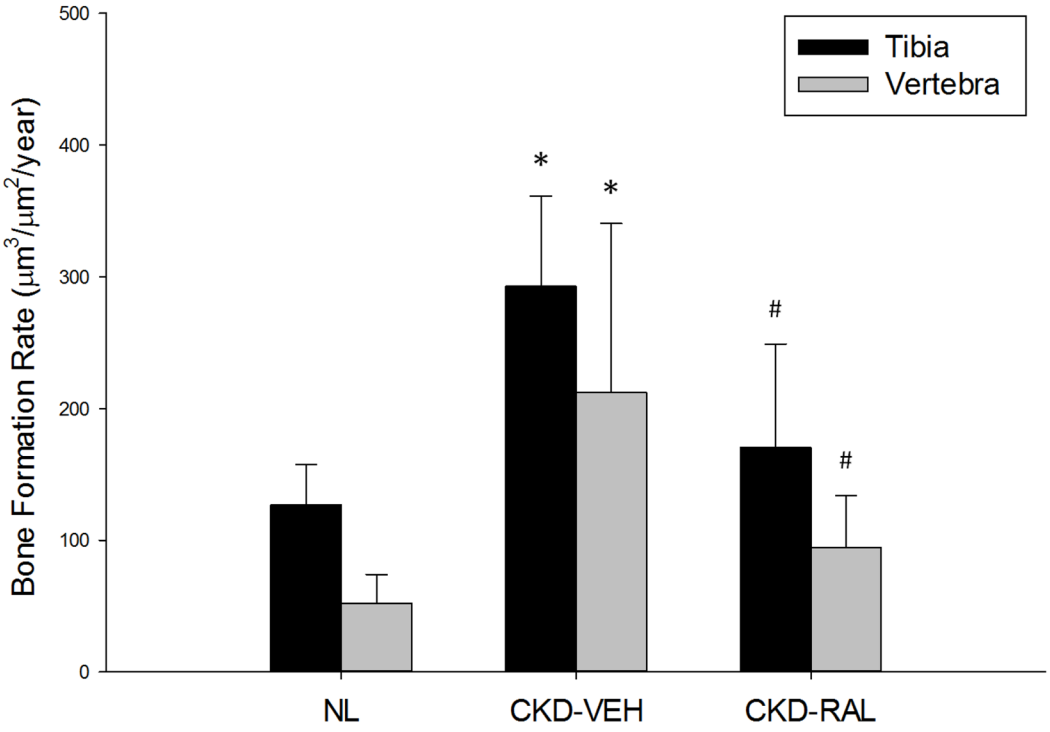

Figure 2.

Bone formation rates in the proximal tibia and caudal lumbar vertebra as determined by dynamic histomorphometry. *, $p<0.05$ compared to NL; #, $p<0.05$ compared to CKD-VEH

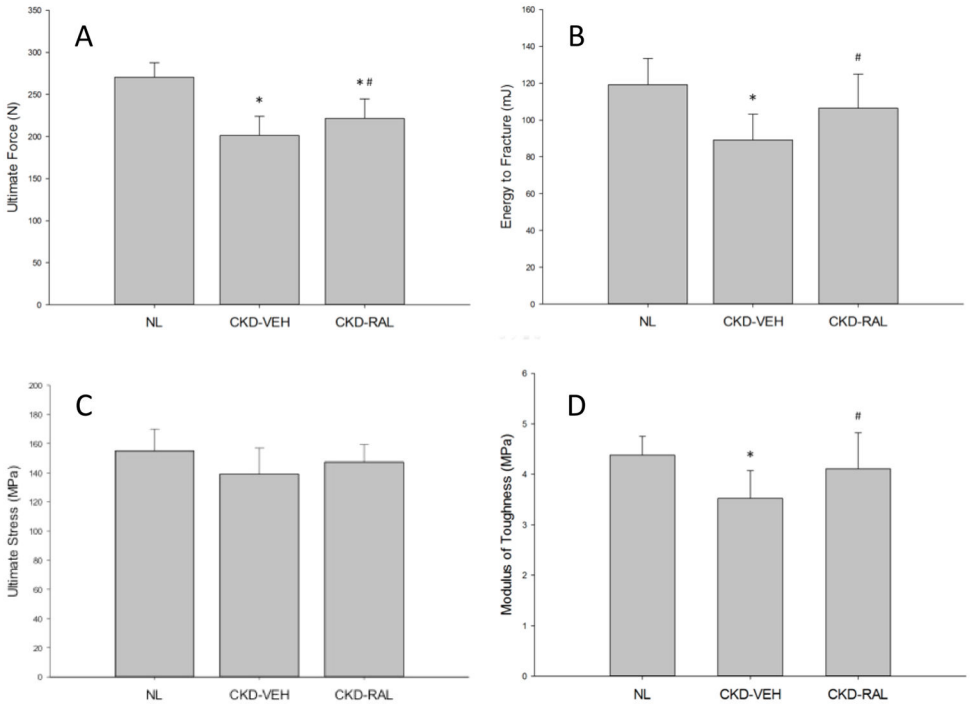

Figure 3.

Structural and apparent material properties of the femur as determined by four-point bending: (a) ultimate load, (b) energy to fracture, (c) ultimate stress, and (d) modulus of toughness. *, $p<0.05$ compared to NL; #, $p<0.05$ compared to CKD-VEH

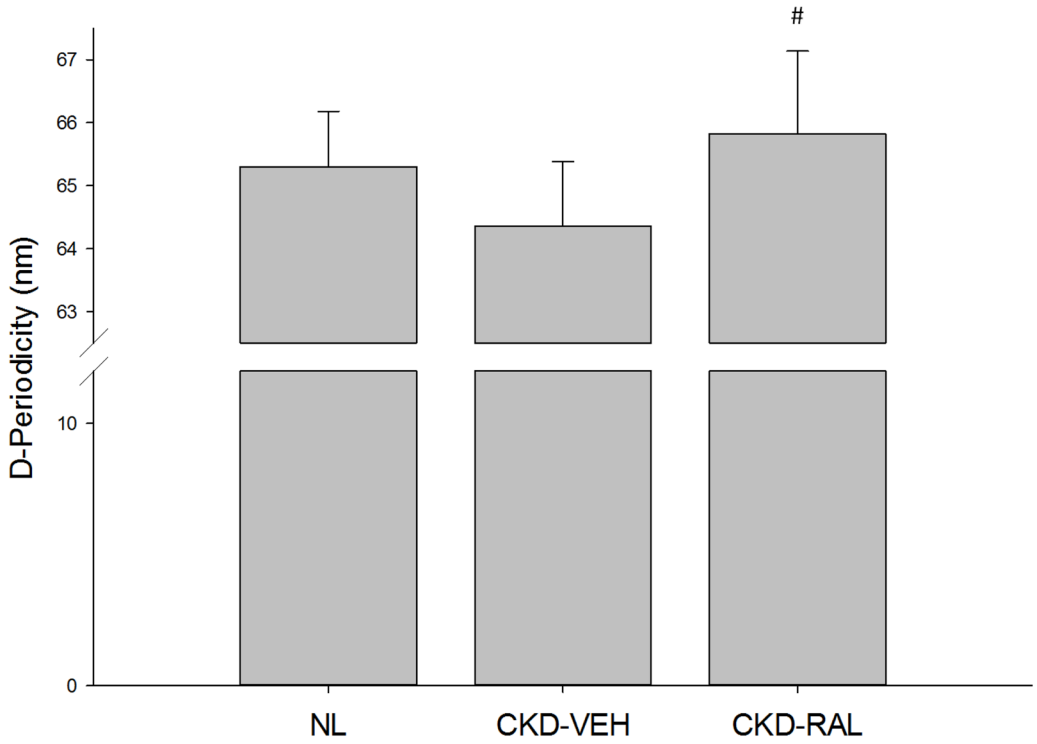

Figure 4.
Collagen fibril D-periodic spacing as determined by AFM imaging. #, $p<0.05$ compared to CKD-VEH

Table 1

Biochemistry

Biochemistry	Normal (n=8)	CKD (Vehicle) (n=9)	CKD (Raloxifene) (n=10)
BUN (mg/dL)§	14.62 ± 1.95	48.32 ± 8.20 *	44.12 ± 5.12 *
Calcium (mg/dL)§	9.979 ± 0.987	11.610 ± 2.323	10.061 ± 2.421
Phosphorus (mg/dL)§	4.527 ± 0.579	6.682 ± 2.408 *	9.700 ± 3.591 *
PTH (pg/mL)¶	181.97 ± 105.05	2194.39 ± 1811.01 *	1257.46 ± 1456.22 *
FGF23 (pg/mL)§	698.36 ± 93.03	2556.83 ± 1401.96 *	6184.88 ± 3403.39 *

§One-Way ANOVA followed by Fisher's LSD tests

¶Kruskal-Wallis test followed Mann-Whitney U tests (with Bonferroni correction)

*vs. Normal

#vs. CKD (Vehicle)

Table 2

MicroCT

Proximal Tibia	**Normal (n=8)**	**CKD (Vehicle) (n=9)**	**CKD (Raloxifene) (n=10)**
BV/TV (%)§	17.04 ± 3.34	11.26 ± 1.51 *	14.9 ± 2.70 #
Tb.Th (mm)¶	0.106 ± 0.010	0.108 ± 0.004	0.103 ± 0.007
Tb.N (1/mm)§	1.611 ± 0.253	1.052 ± 0.150 *	1.451 ± 0.211 #
Tb.Sp (mm)§	0.369 ± 0.044	0.604 ± 0.114 *	0.420 ± 0.055 #
Femoral Diaphysis	Normal (n=8)	CKD (Vehicle) (n=9)	CKD (Raloxifene) (n=10)
Ct.Th (mm)§	0.876 ± 0.037	0.748 ± 0.056 *	0.783 ± 0.039 *
Ct.Ar (mm^2)¶	8.767 ± 0.631	7.324 ± 0.358 *	7.611 ± 0.397 *
I_{ap} (mm^4)¶	15.00 ± 2.59	12.40 ± 0.58 *	12.30 ± 1.35 *
I_{ml} (mm^4)¶	10.23 ± 1.56	7.50 ± 0.59 *	7.86 ± 0.73 *
Ct.Po (%)¶	0.690 ± 0.324	0.948 ± 0.401	0.467 ± 0.274 #
Lumbar Vertebra	Normal (n=8)	CKD (Vehicle) (n=9)	CKD (Raloxifene) (n=10)
BV/TV (%)§	41.88 ± 2.92	30.01 ± 3.98 *	36.27 ± 1.76 *#
Tb.Th (mm)¶	0.119 ± 0.004	0.110 ± 0.007 *	0.108 ± 0.005 *
Tb.N (1/mm)§	3.581 ± 0.258	2.726 ± 0.324 *	3.401 ± 0.129 #
Tb.Sp (mm)§	0.213 ± 0.021	0.280 ± 0.031 *	0.235 ± 0.014 *#
Ct.Th (mm)¶	0.236 ± 0.033	0.170 ± 0.012 *	0.184 ± 0.025 *

§One-Way ANOVA followed by Fisher's LSD tests

¶Kruskal-Wallis test followed Mann-Whitney U tests (with Bonferroni correction)

*vs. Normal

#vs. CKD (Vehicle)

Table 3

Histomorphometry

Tibia	**Normal (n=8)**	**CKD (Vehicle) (n=9)**	**CKD (Raloxifene) (n=10)**
MAR (μm/day)¶	1.305 ± 0.185	2.470 ± 0.569	1.890 ± 0.511
MS/BS (%)§	26.56 ± 5.14	33.32 ± 4.11	23.89 ± 4.75 #
BFR/BS ($\mu m^3/\mu m^2$/year)¶	126.65 ± 31.02	299.62 ± 74.35 *	170.40 ± 78.52 #
Oc.S/BS (%)¶	7.157 ± 1.250	15.739 ± 3.332 *	15.684 ± 6.857 *
N.Oc/BS (1/mm)§	1.966 ± 0.412	4.125 ± 0.785 *	4.134 ± 1.653 *
Vertebra	Normal (n=8)	CKD (Vehicle) (n=9)	CKD (Raloxifene) (n=10)
MAR (μm/day)¶	1.057 ± 0.339	1.983 ± 0.876	1.574 ± 0.400
MS/BS (%)§	13.62 ± 3.98	27.81 ± 5.73 *	16.21 ± 3.73 #
BFR/BS ($\mu m^3/\mu m^2$/year)¶	52.14 ± 21.76	211.94 ± 128.49 *	94.19 ± 39.80 #

§One-Way ANOVA followed by Fisher's LSD tests

¶Kruskal-Wallis test followed Mann-Whitney U tests (with Bonferroni correction)

*vs. Normal

#vs. CKD (Vehicle)

Table 4

Whole Bone Mechanics

Femur	**Normal (n=8)**	**CKD (Vehicle) (n=9)**	**CKD (Raloxifene) (n=10)**
Ultimate Force (N)§	272.08 ± 17.75	204.81 ± 23.20 *	223.44 ± 23.78 *#
Stiffness (N/mm)¶	531.67 ± 47.41	412.96 ± 56.28 *	440.66 ± 30.52 *
Energy to Fracture (mJ)§	119.16 ± 15.33	91.65 ± 14.13 *	107.24 ± 20.86 #
Total Displacement (mm)§	781.56 ± 53.46	745.15 ± 67.76	825.01 ± 95.15
Ultimate Stress (MPa)§	153.81 ± 15.68	143.94 ± 17.93	146.76 ± 13.28
Elastic Modulus (MPa)§	4.649 ± 0.633	5.144 ± 0.971	4.998 ± 0.466
Toughness (MPa)§	4.336 ± 0.382	3.652 ± 0.545 *	4.096 ± 0.814 #
Total Strain (mε)§	50.44 ± 4.48	42.74 ± 4.23 *	47.73 ± 4.97
Mechanics (Vertebra)	Normal (n=8)	CKD (Vehicle) (n=8)	CKD (Raloxifene) (n=10)
Ultimate Force (N)§	256.89 ± 60.01	187.06 ± 48.03 *	179.57 ± 38.63 *
Stiffness (N/mm)§	952.09 ± 314.20	866.74 ± 260.33	854.76 ± 277.85
Energy (mJ)§	46.27 ± 10.60	28.05 ± 8.93 *	26.46 ± 7.33 *
Total Displacement (mm)§	0.445 ± 0.123	0.355 ± 0.062	0.399 ± 0.97
Ultimate Stress (MPa)§	42.49 ± 10.00	38.74 ± 9.16	34.16 ± 7.89
Elastic Modulus (MPa)§	954.37 ± 334.35	1174.00 ± 447.08	1124.68 ± 372.23
Toughness (MPa)§	1.310 ± 0.470	0.924 ± 0.347	0.714 ± 0.135
Total Strain (mε)§	73.84 ± 25.98	58.37 ± 13.51	57.27 ± 12.07

§One-Way ANOVA followed by Fisher's LSD tests

¶Kruskal-Wallis test followed Mann-Whitney U tests (with Bonferroni correction)

*vs. Normal

#vs. CKD (Vehicle)

Table 5

Material Properties – Mechanics

Nanoindentation	**Normal (n=8)**	**CKD (Vehicle) (n=9)**	**CKD (Raloxifene) (n=10)**
Elastic Modulus (GPa)[§]	11.066 ± 2.766	9.666 ± 1.021	13.200 ± 3.345
Hardness (MPa)[¶]	202.62 ± 22.86	192.68 ± 47.35	422.81 ± 291.97 [#]
AFM Indentation	Normal (n=8)	CKD (Vehicle) (n=9)	CKD (Raloxifene) (n=10)
Elastic Modulus (GPa)[§]	52.99 ± 25.81	43.21 ± 16.31	49.25 ± 26.20

[§] One-Way ANOVA followed by Fisher's LSD tests

[¶] Kruskal-Wallis test followed Mann-Whitney U tests (with Bonferroni correction)

[*] vs. Normal

[#] vs. CKD (Vehicle)

Table 6

Material Properties – Composition and Morphology

Raman Spectroscopy	**Normal (n=8)**	**CKD (Vehicle) (n=9)**	**CKD (Raloxifene) (n=10)**
Crystallinity (1/FWHM PO_4^{3-}ν1)§	0.0529 ± 0.0003	0.0534 ± 0.0008	0.0535 ± 0.0005
Carbonate Substitution (CO_3^{2-}ν1/PO_4^{3-}ν1)§	0.247 ± 0.008	0.242 ± 0.013	0.239 ± 0.015
Relative Mineralization (PO_4^{3-}ν1/Amide I)§	2.650 ± 0.332	2.274 ± 0.501	2.384 ± .0422
Collagen Morphology	Normal (n=8)	CKD (Vehicle) (n=9)	CKD (Raloxifene) (n=10)
D-Periodicity (nm)§	65.321 ± 0.946	64.466 ± 1.391	65.438 ± 1.289 #
Collagen Cross-Linking	Normal (n=8)	CKD (Vehicle) (n=9)	CKD (Raloxifene) (n=10)
Pyridinoline per Collagen (mol/mol)§	0.474 ± 0.485	0.223 ± 0.087	0..305 ± 0.079
Deoxypyridinoline per Collagen (mol/mol)§	0.372 ± 0.388	0.203 ± 0.095	0.271 ± 0.088
Pentosidine per Collagen (mmol/mol)§	815.39 ± 621.34	507.06 ± 288.11	617.48 ± 171.46
NMR Spectroscopy	Normal (n=8)	CKD (Vehicle) (n=9)	CKD (Raloxifene) (n=10)
Bound Water (%)¶	18.60 ± 3.61	17.88 ± 4.00	17.34 ± 3.43
Pore Water (%)§	3.829 ± 0.988	5.572 ± 3.567	4.158 ± 0.965

§One-Way ANOVA followed by Fisher's LSD tests

¶Kruskal-Wallis test followed Mann-Whitney U tests (with Bonferroni correction)

*vs. Normal

#vs. CKD (Vehicle)